Original Article: Open Access

DOI: 10.35840/2631-5033/1829

VIBGYOR ePress

International Journal of Earth Science and Geophysics

Synthesis and Luminescent Properties of Monodisperse Spherical RE_2O_3:Eu^{3+} (RE = Gd, Y, Lu, La) Phosphors

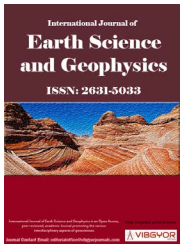

ISSN: 2631-5033

***Jinkai Li*[1*#], *Qi Chen*[1#], *Hongwen Yu*[2*], *Bingqiang Cao*[1] and *Zongming Liu*[1]**

[1]*School of Materials Science and Engineering, University of Jinan, China*

[2]*School of Materials Science and Engineering, Beijing University of Technology, China*

[#]*These two authors contributed to this paper equally.*

Abstract

We studied in detail the effects of morphology and size on the properties of RE_2O_3: Eu^{3+} (RE = Gd, Y, Lu, La) phosphors, the relationship between the coordination environment of Eu^{3+} and fluorescence properties. Through the comparative test of RE_2O_3 (RE = Gd, Y, Lu, La) fluorescent matrix doping with the same activation (Eu^{3+}), the fluorescence properties difference of the four kinds of phosphors was analyzed. Spherical RE_2O_3: Eu^{3+} (RE = Gd, Y, Lu, La) phosphors were successfully prepared by the urea-based homogeneous precipitation method. The particles of these phosphors have perfect spherical shape, narrow size distribution, and non-agglomeration except La_2O_3: Eu^{3+} particles. The $(Gd_{0.95}Eu_{0.05})_2O_3$, $(Y_{0.95}Eu_{0.05})_2O_3$, and $(Lu_{0.95}Eu_{0.05})_2O_3$ samples exhibit strong red emission at ~611 nm ($^5D_0$-$^7F_2$ transition of Eu^{3+}) under excitation wavelength of ~258 nm (CTB of Eu^{3+}, $^8S_{7/2}$-^6I_J transition of Gd^{3+}), but the $(La_{0.95}Eu_{0.05})_2O_3$ sample exhibit weak red emission at ~630 nm ($^5D_0$-$^7F_2$ transition of Eu^{3+}) under excitation wavelength of 290 nm (CTB (charge transfer band) of Eu^{3+}). Among them, $(Gd_{0.95}Eu_{0.05})_2O_3$ phosphors have the best fluorescent properties due to the energy transfer of Gd^{3+}→Eu^{3+} which further enhance the red emission at ~611 nm ($^5D_0$-$^7F_2$ transition of Eu^{3+}). All the $(RE_{0.95}Eu_{0.05})_2O_3$ phosphors in this work have similar CIE chromaticity coordinates (~0.65 ± 0.01, ~0.34 ± 0.01), high color purity, and similar fluorescence lifetimes (~1.70 ± 0.1). Therefore, the excellent type of $(Gd_{0.95}Eu_{0.05})_2O_3$ phosphors in this work will be expected to be widely used in lighting and display areas.

Keywords

RE_2O_3: Eu^{3+} phosphors, Urea-based homogeneous precipitation, Luminescence property

Introduction

Recently, RE_2O_3 (RE = Gd, Y, Lu, La) have been interestingly studied owing to their excellent physical and chemical properties, monodisperse spherical particle morphology and potential applications as matrix in the fields of luminescence devices [1-9]. Eu^{3+} activated RE_2O_3 is well-known red-emitting phosphors widely used in the white LEDs [10-13], and displays such as plasma display panels (PDP) [14], field emission displays (FED) [3,15-21], and

***Corresponding author:** *Dr. Jinkai Li, School of Materials Science and Engineering, University of Jinan, Jinan, Shandong 250022, China, Tel: +86-531-82765894; Hongwen Yu, School of Materials Science and Engineering, Beijing University of Technology, China*

Accepted: November 18, 2019; **Published:** November 20, 2019

ISSN 2631-5033

Citation: Li J, Chen Q, Yu H, Cao B, Liu Z (2019) Synthesis and Luminescent Properties of Monodisperse Spherical RE_2O_3:Eu^{3+} (RE = Gd, Y, Lu, La) Phosphors. Int J Earth Sci Geophys 5:029

cathode-ray tubes (CRT) [22].

Based on the above situation, we want to study the fluorescence properties of RE_2O_3: Eu^{3+} (RE = Gd, Y, Lu, La) phosphors by analyzing the morphology and size of powders, and the coordination environment of Eu^{3+}. However, the researchers are more inclined to fully study a single type of phosphor, including the synthesis and fluorescence properties of the phosphor. There is no research report on the comparative analysis of properties of RE_2O_3: Eu^{3+} (RE = Gd, Y, Lu, La) phosphors. In addition, we want to compare and analyze the fluorescent powders synthesized by the same activator Eu^{3+} with RE_2O_3 (RE = Gd, Y, Lu, La) fluorescent matrix, and it is expected to have a more direct comparison of its fluorescence performance, and the application prospect of each phosphor is analyzed. Among which, the phosphors possess high color purity (> 90%) is needed which is an important performance of phosphor used in display field [23].

Therefore, the situation and fluorescence properties of RE_2O_3: Eu^{3+} (RE = Gd, Y, Lu, La) was systematically studied and analyzed in this work. This is mainly for the three following reasons: (1) RE_2O_3: Eu^{3+} phosphor particles have strong luminescence intensity owing to good dispersion and sphericity [24,25]; (2) Eu^{3+} as one of the most widely red phosphor activator, was usually used in a lot of studies on the fluorescence properties in single matrix, but there are few studies on the difference of fluorescence properties of Eu^{3+} in different matrices. Furthermore, the Gd^{3+} may sensitize red emission of Eu^{3+} ($^5D_0$-$^7F_{1,2}$ transition of Eu^{3+}) via efficient Gd^{3+}→Eu^{3+} energy transfer, which can enhance the red emission of Eu^{3+} [26-32]; (3) Although the synthetic methods of rare-earth oxide phosphors are diversified, the solid phase method is much more studied than the chemical liquid phase method, so the chemical liquid phase method is used in this work.

Experimental Procedure

In this paper, the precursor was prepared by the urea-based homogeneous precipitation method, and then calcined at 1273 K to obtain the RE_2O_3: Eu^{3+} (RE = Gd, Y, Lu, La) phosphors. Crystalline phases of the RE_2O_3: Eu^{3+} (RE = Gd, Y, Lu, La) phosphors had been examined and confirmed by XRD. Particle size and morphology parameters of the phosphors were verified by FE-SEM. The luminescent properties were investigated by the PLE/PL spectroscopy and decay kinetics analysis. Therefore, we gave a detailed description of the synthesis, crystalline phases, morphology and luminescent properties of the RE_2O_3: Eu^{3+} (RE = Gd, Y, Lu, La) phosphors.

The raw materials used in this work are rare-earth oxides (Gd_2O_3, Y_2O_3, Lu_2O_3, La_2O_3 and Eu_2O_3, 99.99% pure, Huizhou Ruier Rare Chemical Hi-Tech Co. Ltd., Huizhou, China), $CO(NH_2)_2{\cdot}12H_2O$ (AR, Sinopharm Chemical Reagent Co. Ltd., Shanghai, China), and HNO_3 (AR, Sinopharm Chemical Reagent Co. Ltd., Shanghai, China). All the reactants were directly involved in the reaction and need not be further purified.

Rare-earth oxides were dissolved in hot nitric (353 K) acid to obtain rare-earth nitrates. The mother salt solution was achieved through mixing the $RE(NO_3)_3$ solutions according to the formula of $(RE_{1-x}Eu_x)_2O_3$ (RE = Gd, Y, Lu, La, and x = 0.05). The CH_4N_2O (with 40 times the molar quantities of cations) was added in the mother solution, and the total volume was kept at 500 mL. The mixed solutions were firstly homogenized under stirring for 60 min at 298 K and then heated to 363 ± 1 K within 60 min. The precipitation was assembled through centrifuge after aging treatment for 2 h at 363 ± 1 K, and washed repeatedly with deionized water and alcohol to remove impurities. The wet precipitation was dried in air at 353 K for 24 h. The precursor was finally calcined at 1273 K for 4 h to obtain the resultant particles. Compared to the traditional synthesized methods, such as solid-state reaction [22], co-precipitation [8,26,32], hydrothermal method [2,3,17,27], and so on, the $(RE_{0.95}Eu_{0.05})_2O_3$ (RE = Gd, Y, Lu) powders synthesized by urea-based homogeneous precipitation method possesses good dispersion and perfect spherical shape [21,23,25].

Crystalline phases were characterized by powder X-ray diffraction (D8-ADVANCE, BRUKER Co. Ltd., Germany) using nickel-filtered CuKα radiation under 40 kV/40 mA and a scanning speed of XRD diffraction angle (2ϑ) is 4°/min; Particle morphologies were observed via FE-SEM (QUNATAFEG-250, FEI Co. Ltd., USA); The photoluminescence spectra of the $(RE_{1-x}Eu_x)_2O_3$ phosphors were measured under excitation light of a 150 W Xe lamp on the fluorescence spectrophotometer (FP-6500, JASCO Co. Ltd., Japan).

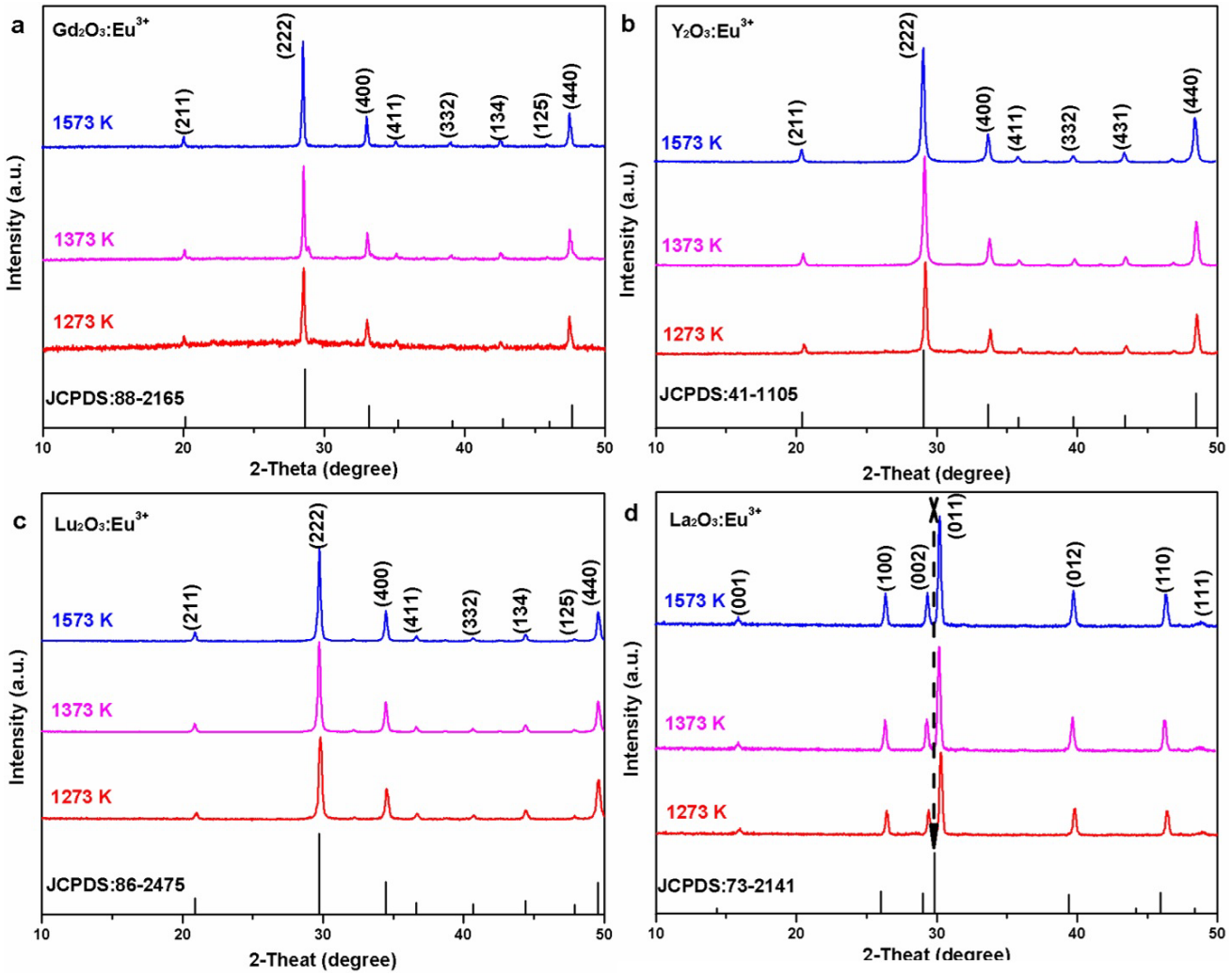

Figure 1: The XRD patterns of $(RE_{0.95}Eu_{0.05})_2O_3$ (RE = Gd (a), Y (b), Lu (c), La (d)) precursor powders calcined at 1273 K, respectively.

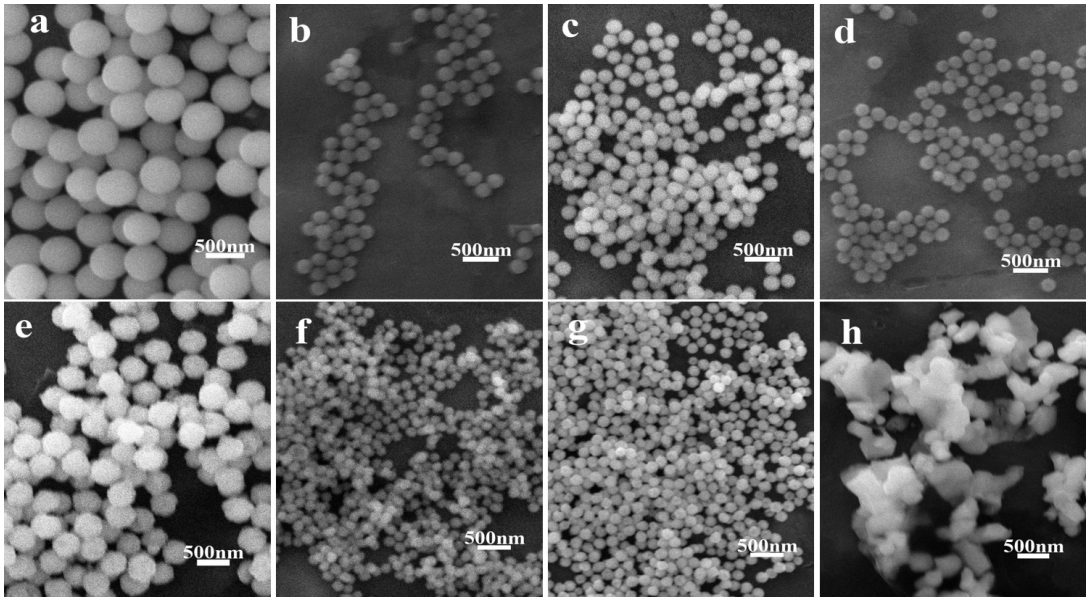

Figure 2: Particle morphologies of the $(RE_{0.95}Eu_{0.05})_2O_3$ precursor (Gd (a), Y (b), Lu (c), La (d)) and the precursors calcining at 1273 K for 4h to obtain the resultant particles (Gd (e), Y (f), Lu (g), La (h)).

Citation: Li J, Chen Q, Yu H, Cao B, Liu Z (2019) Synthesis and Luminescent Properties of Monodisperse Spherical $RE_2O_3:Eu^{3+}$ (RE = Gd, Y, Lu, La) Phosphors. Int J Earth Sci Geophys 5:029

Result and Discussion

Figure 1 shows the XRD patterns of $(RE_{0.95}Eu_{0.05})_2O_3$ (RE = Gd, Y, Lu, La) precursors calcined at 1273 K. It can be seen that all of the samples calcined at 1273 K have sharp characteristic peaks. The pure phase $(Gd_{0.95}Eu_{0.05})_2O_3$, $(Y_{0.95}Eu_{0.05})_2O_3$, and $(Lu_{0.95}Eu_{0.05})_2O_3$ were formed indicating that the addition of Eu^{3+} did not alter the crystal structure, but the $(La_{0.95}Eu_{0.05})_2O_3$ diffraction peaks shift towards large angle owing to the smaller radius of Eu^{3+} than La^{3+}. The radius of Gd^{3+}, Y^{3+}, Lu^{3+}, La^{3+} and Eu^{3+} are 1.053 Å, 1.019 Å, 0.977 Å, 1.16 Å and 1.066 Å, respectively. Because the ion radius of La^{3+} is larger than that of Eu^{3+}, the lattice of this phosphor shrank when Eu^{3+} replaces the La^{3+} in the cell, resulting in the drifts of XRD diffraction peak to a large angle.

The scanning electron microscopy morphologies of the $(RE_{0.95}Eu_{0.05})_2O_3$ (RE = Gd, Y, Lu, La) precursors and precursors calcining at 1273 K were presented in Figure 2. It can be seen that all four precursors have excellent spherical morphology and dispersity indicating that the urea-based homogeneous precipitation method can stably obtain the samples of this morphology. The average particle size of $(Gd_{0.95}Eu_{0.05})_2O_3$ (a), $(Y_{0.95}Eu_{0.05})_2O_3$ (b), $(Lu_{0.95}Eu_{0.05})_2O_3$ (c), and $(La_{0.95}Eu_{0.05})_2O_3$ (d) precursors were ~500 nm, ~170 nm, ~230 nm, and ~280 nm, respectively. The difference in particle size among the four precursors is mainly due to different nucleation density. By comparing the FE-SEM photos (e, f, g), the former three precursors calcining at 1273 K can maintain excellent monodisperse spherical morphology, but the phosphor particle of $(La_{0.95}Eu_{0.05})_2O_3$ (h) was sintered. The doping of Eu^{3+} makes the lattice structure of $(La_{0.95}Eu_{0.05})_2O_3$ severe shrinkage, leading to many defects in precursor of $(La_{0.95}Eu_{0.05})_2O_3$, which makes the spherical precursor unable to maintain the original morphology at 1273 K.

Figure 3 shows the excitation spectra of $(RE_{0.95}Eu_{0.05})_2O_3$ (RE = Gd, Y, Lu, La) monitoring at 611 nm, 610 nm, 610 nm and 626 nm emission (the $^5D_0$-$^7F_2$ transition of Eu^{3+}), respectively. $(Gd_{0.95}Eu_{0.05})_2O_3$, $(Y_{0.95}Eu_{0.05})_2O_3$ and $(Lu_{0.95}Eu_{0.05})_2O_3$ phosphors have a broad PLE band at ~258 nm and $(La_{0.95}Eu_{0.05})_2O_3$ phosphors is at ~290 nm. Both of

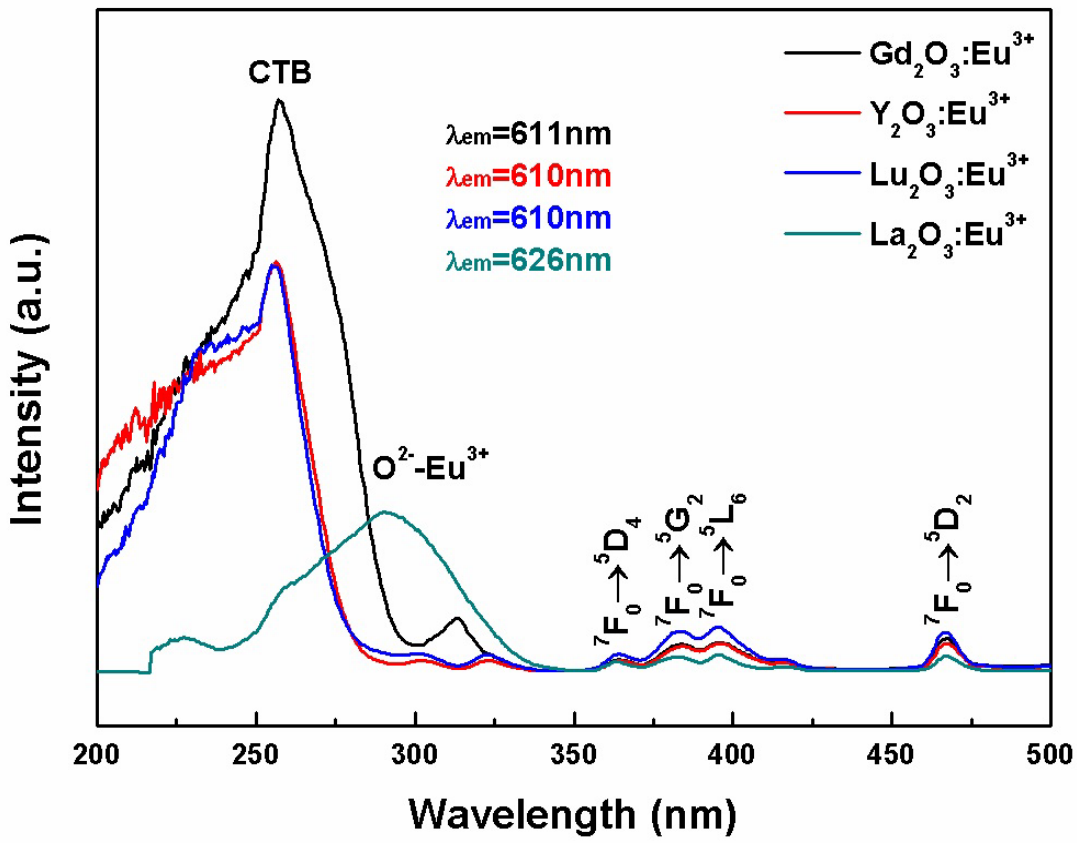

Figure 3: A comparison of the PLE behaviors of the $(Gd_{0.95}Eu_{0.05})_2O_3$, $(Y_{0.95}Eu_{0.05})_2O_3$, $(Lu_{0.95}Eu_{0.05})_2O_3$, and $(La_{0.95}Eu_{0.05})_2O_3$ phosphors, the PLE spectra were taken by monitoring the 611 nm, 610 nm, 610 nm, and 626 nm emissions, respectively.

Citation: Li J, Chen Q, Yu H, Cao B, Liu Z (2019) Synthesis and Luminescent Properties of Monodisperse Spherical RE_2O_3:Eu^{3+} (RE = Gd, Y, Lu, La) Phosphors. Int J Earth Sci Geophys 5:029

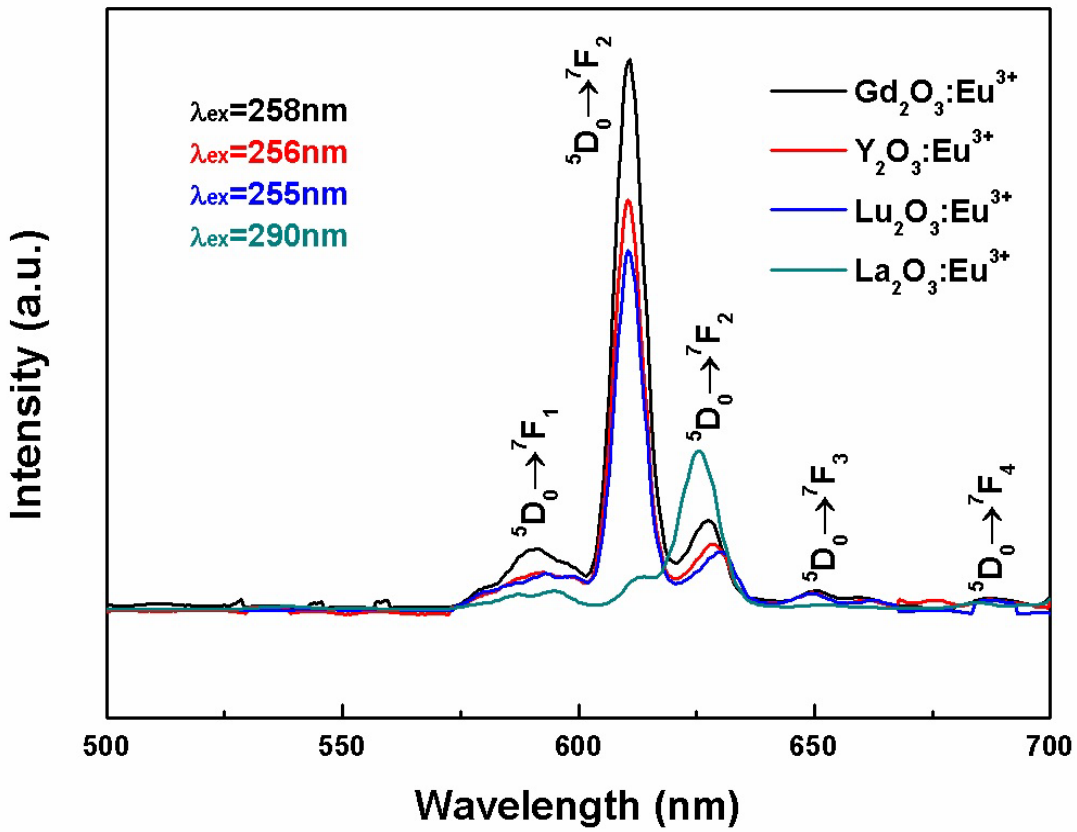

Figure 4: The emission spectra of $(Gd_{0.95}Eu_{0.05})_2O_3$, $(Y_{0.95}Eu_{0.05})_2O_3$, $(Lu_{0.95}Eu_{0.05})_2O_3$, and $(La_{0.95}Eu_{0.05})_2O_3$ phosphors under 258 nm, 256 nm, 255 nm and 290 nm excitation, respectively.

the two excitation peaks are due to a CTB (charge transfer band), namely, the electronic transition from the 2*p* orbital of O^{2-} to the 4*f* orbital of Eu^{3+} activators [33]. The electronegativity of Gd, Y, Lu and La are 1.2, 1.22, 1.27 and 1.1, respectively. Due to the electronegativity of La is lower than that of Gd, Y and Lu, La has weaker ability to attract electrons caused the excitation peak of $(La_{0.95}Eu_{0.05})_2O_3$ phosphors to shift towards large angle. However, the irregular morphology of $(La_{0.95}Eu_{0.05})_2O_3$ phosphor particles leads to the weakest intensity of excitation peak. It is noteworthy that the strongest excitation peak at ~258 nm stems from the characteristic transition of $(Gd_{0.95}Eu_{0.05})_2O_3$ and $^8S_{7/2}$-^6I_J of Gd^{3+} overlapped, implying the $Gd^{3+}\rightarrow Eu^{3+}$ energy transfer. As marked in the figure, the other bands were mainly *f*-*f* transition of Eu^{3+} located at ~362 nm ($^7F_0$-$^5D_4$), ~387 nm ($^7F_0$-$^5G_2$), ~394 nm ($^7F_0$-$^5L_6$) and ~465 nm ($^7F_0$-$^5D_2$), respectively.

According to the PLE spectra, the optimum excitation wavelength was determined. Based on this, the emission spectra of the $(RE_{0.95}Eu_{0.05})_2O_3$ (RE = Gd, Y, Lu, La) phosphor were achieved under the optimum wavelength shown in Figure 4. The four typical emission bands originating from electron transition of Eu^{3+} ion can be noticed: $^5D_0$-$^7F_1$ (~587 nm), $^5D_0$-$^7F_2$ (~611 nm, the strongest), $^5D_0$-$^7F_3$ (~654 nm), and $^5D_0$-$^7F_4$ (~689 nm) [7,10-13,19,22-26,32,33]. Furthermore, the weak emission peak at ~630 nm is also derived from the $^5D_0$-$^7F_2$ transition of Eu^{3+} ion. The 611 nm emission intensity of $(Gd_{0.95}Eu_{0.05})_2O_3$ is higher than other samples due to three reasons: (1) The efficient $Gd^{3+}\rightarrow Eu^{3+}$ energy transfer enhanced the red emission of $(Gd_{0.95}Eu_{0.05})_2O_3$ as revealed by PLE (Figure 3). (2) Due to the electronegativity of Gd is lower than that of Y and Lu, Gd has weaker ability to attract electrons and lower transferred energy. However, the luminescence intensity of $(La_{0.95}Eu_{0.05})_2O_3$ phosphor at 626 nm is weakest due to it has irregular morphology. (3) The surface defects of $(Gd_{0.95}Eu_{0.05})_2O_3$ phosphor particle are less than other samples owing to maximum particle size and minimal surface area. Besides, the strongest emission peak (626 nm) of $(La_{0.95}Eu_{0.05})_2O_3$ shift towards large angle compared with other three kinds of phosphors implying the elec-

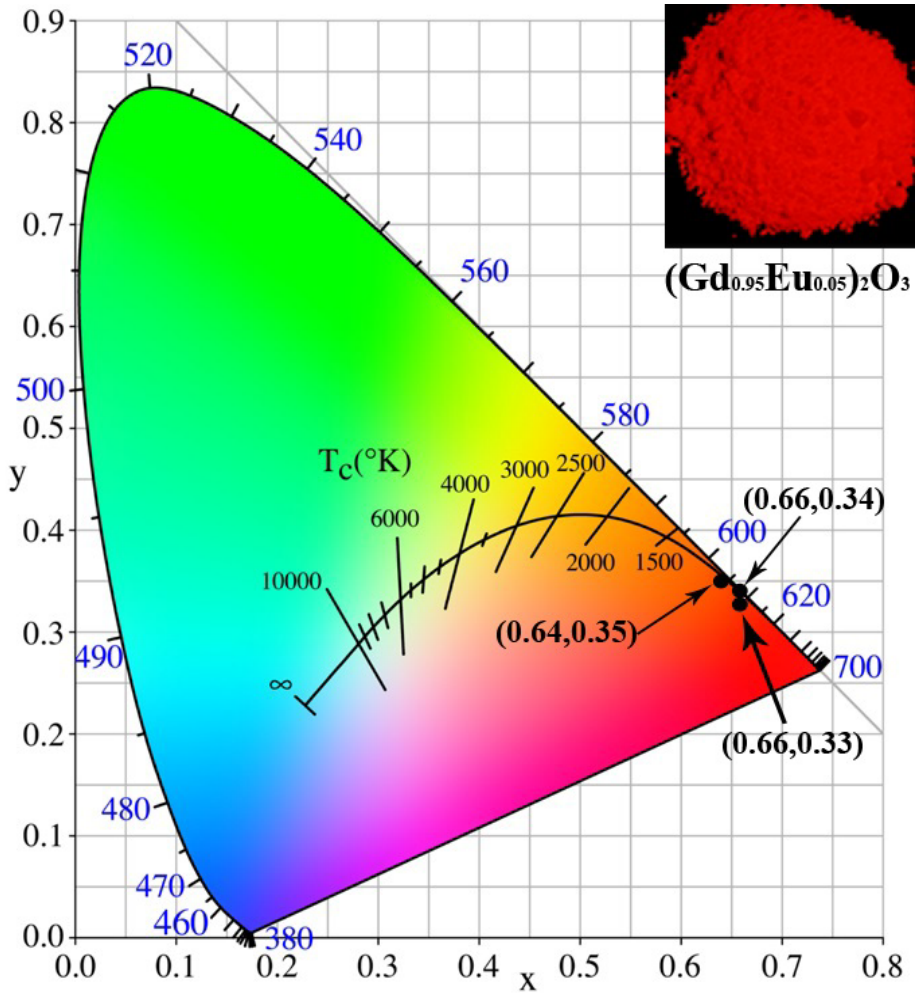

Figure 5: CIE chromaticity coordinate and color temperature of the $(RE_{0.95}Eu_{0.05})_2O_3$ (RE = Gd, Y, Lu, La) phosphors calcined at 1000 °C. Inset is the appearance of $(Gd_{0.95}Eu_{0.05})_2O_3$ emission excited at 254 nm with a hand-held UV lamp.

tronegativity of La is lower than that of Gd, Y and Lu. On the other side, it is well-known that the Eu^{3+} occupy S_6 and C_2 sites in Ln_2O_3 oxides. The different spectra between Gd_2O_3, Lu_2O_3, Y_2O_3 and La_2O_3 indicate the different Eu^{3+} sites in these oxides.

The CIE chromaticity coordinates for the emission of the $(RE_{0.95}Eu_{0.05})_2O_3$ (RE = Gd, Y, Lu, La) phosphors under the respective wavelength excitation are shown in Figure 5. The CIE chromaticity coordinate of $(Gd_{0.95}Eu_{0.05})_2O_3$ is determined to be (0.64, 0.35) with vivid red color via 254 nm UV excitation from a hand-held UV lamp, as shown in inset. The chromatic coordinate of $(Y_{0.95}Eu_{0.05})_2O_3$ was calculated to be (0.66, 0.33), and the samples of $(Lu_{0.95}Eu_{0.05})_2O_3$ and $(La_{0.95}Eu_{0.05})_2O_3$ were calculated to have the uniform color coordinates (*x*, *y*) of (0.66, 0.34). The corresponding color temperature was calculated according to the following formulas:

$$T = -437n^3 + 3601n^2 - 6861n + 5514.31 \quad (1)$$

and

$$n = (x - 0.332)/(y - 0.1858) \quad (2)$$

where *T* is color temperature of phosphors, (*x*, *y*) is the color coordinate of the light source, *n* is variable.

The color temperatures of the samples were ~2768 K ($Gd_2O_3:Eu^{3+}$), ~3806 K ($Y_2O_3:Eu^{3+}$), and ~3390 K ($La_2O_3:Eu^{3+}$, $Lu_2O_3:Eu^{3+}$), respectively. Further observation is that all the $(RE_{0.95}Eu_{0.05})_2O_3$ (RE = Gd, Y, Lu, La) phosphors have similar CIE chromaticity coordinate of (0.65 ± 0.01, 0.34 ± 0.01), and $(Gd_{0.95}Eu_{0.05})_2O_3$ has a lower color temperature.

The color purity is an important property of the phosphor chromaticity property, and we can use the following formulas to calculate the color purity:

$$Colorpurity = \frac{\sqrt{(x-x_i)^2+(y-y_i)^2}}{(x_d-x_i)^2+(y_d-y_i)^2}\times 100\% \quad (3)$$

where (x, y) is the color coordinate of the light source, (x_i, y_i) is the CIE of an equal-energy illuminant with a value of (0.3333, 0.3333), and (x_d, y_d) is the chromaticity coordinate corresponding to the dominant wavelength of the light source. Through consulting literature, we can obtain the (x_d, y_d) chromaticity coordinate of $(Gd_{0.95}Eu_{0.05})_2O_3$ and $(La_{0.95}Eu_{0.05})_2O_3$ were (0.6658, 0.3340) and (0.7006, 0.2993), respectively, and the (x_d, y_d) color coordinates of $(Y_{0.95}Eu_{0.05})_2O_3$ and $(Lu_{0.95}Eu_{0.05})_2O_3$ are the same as those of $(Gd_{0.95}Eu_{0.05})_2O_3$. By substituting the coordinates of (x, y), (x_i, y_i), and (x_d, y_d) in Eq. (3), the color purities of $(Gd_{0.95}Eu_{0.05})_2O_3$, $(Y_{0.95}Eu_{0.05})_2O_3$, $(Lu_{0.95}Eu_{0.05})_2O_3$ and $(La_{0.95}Eu_{0.05})_2O_3$ are determined to be 92.38%, 98.26%, 98.28% and 88.59% respectively. The results show that $(RE_{0.95}Eu_{0.05})_2O_3$ series phosphors have excellent red emission and high color purity.

The PL thermal properties of phosphors for LEDs are necessary technological parameters. Thus, the effect of temperature on luminescence and activation energy of thermal quenching were studied via the PL spectra in 298-573 K temperature range, the results were shown in Figure 6a. The shape and positions of PL bands do not change with the temperature variation, but the emission intensity of Eu^{3+} in $(Gd_{0.95}Eu_{0.05})_2O_3$ decreases with the temperature increasing. Since the energy transfer effect is also affected by temperature, the rate of decline is different. The decrease of emission intensity is due to the thermal quenching caused by the thermal activation of the crossing point between the ground and the excited state. The emission intensities of Eu^{3+} at 373 K could retain about 99.30% of their corresponding initial values at 298 K. In order to investigate the temperature-dependent thermal quenching phenomenon, the activation energy can be achieved using the Arrhenius equation:

$$\ln\left(\frac{I_0}{I}-1\right) = \ln A - \frac{E_\alpha}{kT} \quad (4)$$

where E_α and T represent the objective activation energy and temperature (K), respectively. A is a constant and k is the Boltzmann constant (8.626×10^{-5} eV). I_0 is the integrated emission intensity at room temperature and I is the integrated emission intensity at differently operated temperatures. The $\ln(I_0/I\text{-}1)$ versus $1/kT$ activation energy graph for thermal quenching of the $(Gd_{0.95}Eu_{0.05})_2O_3$ phosphor is plotted in Figure 6b, which shows that the slope of the best fitting line is -0.4631, thus the activation energy E_α is approximately 0.4631 eV. The relatively high activation energy achieved in this work indicates that it possesses good thermal stability and is an excellent candidate for application in LEDs.

Figure 7 shows the decay kinetics for 610-626

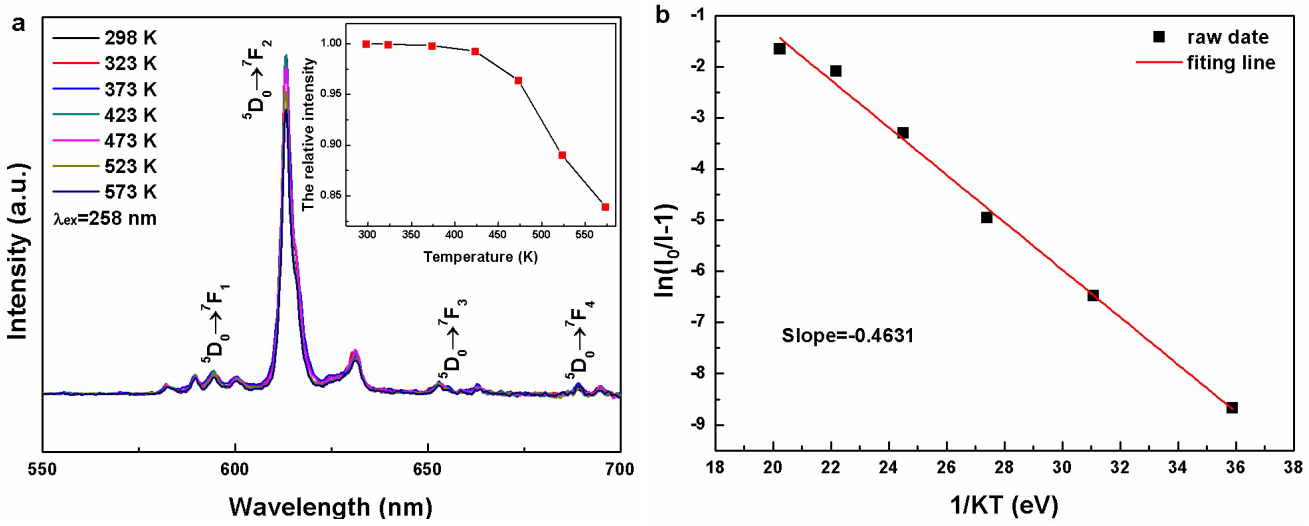

Figure 6: a) The temperature-dependence of the PL spectra of the $(Gd_{0.95}Eu_{0.05})_2O_3$ phosphors; b) Linear relationship of $\ln(I_0/I\text{-}1)$ versus $1/kT$ for thermal quenching of the $(Gd_{0.95}Eu_{0.05})_2O_3$ sample. The inset in (a) is the relative intensity of the 611 nm emission as a function of the Eu^{3+} content, normalized to that of the room temperature (298 K).

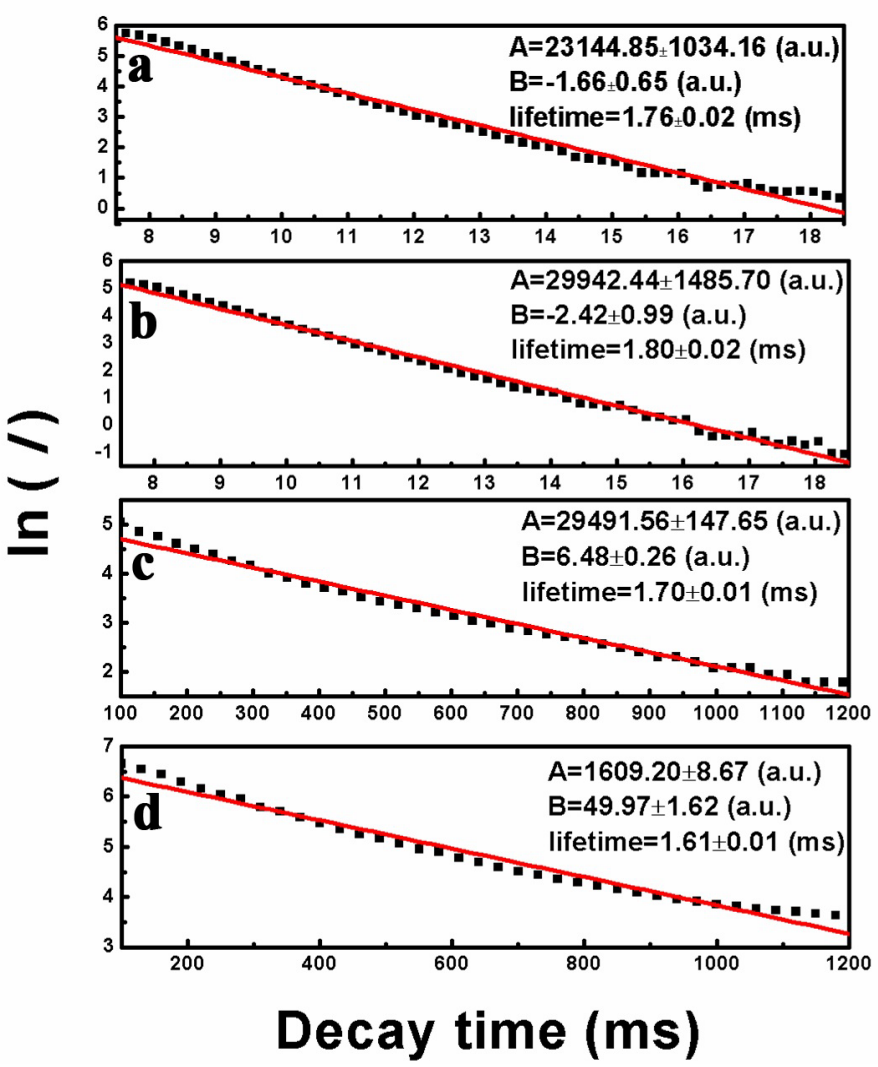

Figure 7: Fluorescence decay kinetics for $(RE_{0.95}Eu_{0.05})_2O_3$ (RE = Gd (a), Y (b), Lu (c), La (d)) phosphors calcined at 1273 K.

nm emission of the $(RE_{0.95}Eu_{0.05})_2O_3$ phosphors calcined at 1273 K. The decay curve can be fitted via the formula:

$$I = A\exp\left(-t/\tau_R\right) + B \quad (5)$$

where I is the relative fluorescence intensity, t is the fluorescence lifetime, τ_R is the decay time. A and B are constants. Figure 7a, Figure 7b, Figure 7c and Figure 7d displays the lifetime value of Gd, Y, Lu and La, which are 1.76 ms, 1.80 ms, 1.70 ms and 1.61 ms, respectively. The results show that the fluorescence lifetimes of $(RE_{0.95}Eu_{0.05})_2O_3$ phosphors are similar.

Conclusions

The $(RE_{0.95}Eu_{0.05})_2O_3$ phosphors have been synthesized by the urea-based homogeneous precipitation method at 1273 K. The $(RE_{0.95}Eu_{0.05})_2O_3$ (RE = Gd, Y, Lu) powders with uniform particle morphology exhibit strong red emission at ~611 nm ($^5D_0$-$^7F_2$ transition of Eu^{3+}) under excitation wavelength of ~258 nm (CTB of Eu^{3+}, $^8S_{7/2}$-^6I_J transition of Gd^{3+}), but the $(La_{0.95}Eu_{0.05})_2O_3$ powders were sintered and exhibit weak red emission at ~630 nm ($^5D_0$-$^7F_2$ transition of Eu^{3+}) under excitation wavelength of 290 nm (CTB of Eu^{3+}). Furthermore, the presence of Gd^{3+} excitation bands on the PLE spectra monitoring the Eu^{3+} emission directly proves $Gd^{3+}\rightarrow Eu^{3+}$ energy transfer, which can further enhance the red emission of the $(Gd_{0.95}Eu_{0.05})_2O_3$ phosphors. All the $(RE_{0.95}Eu_{0.05})_2O_3$ (RE = Gd, Y, Lu, La) phosphors in this work have similar CIE chromaticity coordinates at (~0.65 ± 0.01, ~0.34 ± 0.01). And the color temperatures and color purities of the samples were ~2768 K, 92.38% (Gd_2O_3:Eu^{3+}), ~3806 K, 98.26%

(Y_2O_3:Eu^{3+}), ~3390 K, 98.28% (Lu_2O_3:Eu^{3+}), ~3390 K and 88.59% (La_2O_3:Eu^{3+}), respectively. Fluorescence decay analysis found that the $(RE_{0.95}Eu_{0.05})_2O_3$ (RE = Gd, Y, Lu, La) phosphors in this work have similar lifetime (~1.70 ± 0.1). Therefore, the $(Gd_{0.95}Eu_{0.05})_2O_3$ phosphors will be widely used in lighting and display fields. In general, we studied more deeply and comprehensively the relationship between the morphology and fluorescence properties of $(RE_{0.95}Eu_{0.05})_2O_3$ (RE = Gd, Y, Lu, La) phosphors than the previous reported results.

Acknowledgements

This work was supported in part by the National Natural Science Foundation of China (No. 51402125 and 51602042), China Postdoctoral Science Foundation (No. 2017M612175), the Special Fund for the Postdoctoral Innovation Project in Shandong Province (No. 201603061), the Research Fund for the Doctoral Program of University of Jinan (No. XBS1447), the Natural Science Foundation of University of Jinan (No. XKY1515), the Science Foundation for Post Doctorate Research from the University of Jinan (No. XBH1607), the Natural Science Foundation of Shandong Province (No. ZR2016QL004).

References

1. BF Qian, HF Zou, DY Meng, XQ Zhou, YH Song, et al. (2018) Columnar Gd_2O_3:Eu^{3+}/Tb^{3+} phosphors: Preparation, luminescence properties and growth mechanism. Cryst Eng Comm 20: 7322-7328.
2. Kumar, MHM Couto, SP Tiwari, K Kumar, JCG Esteves da Silva (2018) Effect of pH of precursor on up/down-conversion and cathodoluminescence of Gd_2O_3:Ho^{3+}/Yb^{3+} phosphor and magneto-optic studies. Chemistry Select 3: 10566-10573.
3. R Priya, OP Pandey (2018) Hydrothermal synthesis of Eu^{3+}-doped Gd_2O_3 nanophosphors and its Judd-Ofelt analysis. Vacuum 156: 283-290.
4. M Haase, H Schaefer (2011) Upconverting nanoparticles. Angew Chem Int Edit 50: 5808-5829.
5. R Bazzi, MA Flores, C Louis, K Lebbou, W Zhang, et al. (2004) Synthesis and properties of europium-based phosphors on the nanometer scale: Eu_2O_3, Gd_2O_3:Eu, and Y_2O_3:Eu. J Colloid Interf Sci 273: 191-197.
6. L Robindro Singh, RS Ningthoujam, V Sudarsan, I Srivastava, S Dorendrajit Singh, et al. (2008) Luminescence study on Eu^{3+} doped Y_2O_3 nanoparticles: Particle size, concentration and core-shell formation effects. Nanotechnology 19: 055201.
7. Yang P, Gai S, Liu Y, Wang W, Li C, et al. (2011) Uniform hollow Lu_2O_3:Ln (Ln = Eu^{3+}, Tb^{3+}) spheres: Facile synthesis and luminescent properties. Inorg Chem 50: 2182-2190.
8. L Li, HH Lin, XQ Zhao, YJ Wang, XJ Zhou, et al. (2014) Effect of Yb^{3+} concentration on upconversion luminescence in Yb^{3+}, Tm^{3+} co-doped Lu_2O_3 nanophosphors. J Alloy Compd 586: 555-560.
9. R Dey, VK Rai (2013) Yb^{3+} sensitized Er^{3+} doped La_2O_3 phosphor in temperature sensors and display devices. Dalton T 43: 111-118.
10. C Ma, XD Li, M Zhang, SH Liu, JG Li, et al. (2018) Synthesis of equal-sized Y_2O_3: Bi, Eu mono-spheres and their color-tunable photoluminescence and thermal quenching properties. Ceram Int 44: 18462-18470.
11. T Alammar, J Cybinska, PS Campbell, AV Mudring (2016) Sonochemical synthesis of highly luminescent Ln_2O_3:Eu^{3+} (Y, La, Gd) nanocrystals. J Lumin 169: 587-593.
12. T Selvalakshmi, S Sellaiyan, A Uedono, AC Bose (2015) Investigation on photoluminescence, electrical and positron lifetime of Eu^{3+} activated Gd_2O_3 phosphors. Mater Chem Phys 166: 73-81.
13. RGA Kumar, S Hata, K Ikeda, KG Gopchandran (2015) Luminescence dynamics and concentration quenching in $Gd_{2-x}Eu_xO_3$ nanophosphor. Ceram Int 41: 6037-6050.
14. L Amidani, K Korthout, JJ Joos, M van der Linden, HF Sijbom, et al. (2017) Oxidation and luminescence quenching of europium in $BaMgAl_{10}O_{17}$ blue phosphors. Chem Mater 29: 10122-10129.
15. MX Li, Y Feng, QY Tian, WJ Yao, L Liu, et al. (2018) Tunable and ultra-stable UV light-switchable fluorescent composites for information hiding and storage. Dalton T 47: 11264-11271.
16. K Lingadurai, B Sundarakannan, ER Nagarajan, H Kominami, Y Nakanishi, et al. (2016) Low voltage cathode-luminescent properties of Zn co-doped Y_2O_3: Eu red phosphor. J Lumin 177: 249-253.
17. L Zhou, XH Yang, CX Li, J Yang, Y Luo, et al. (2015) Facile Template free synthesis and tunable RGB luminescent properties of Ln^{3+}-doped yttrium oxide nanospheres. ECS J Solid State Sc 4: 14-19.
18. JS Souris, SH Cheng, C Pelizzari, NT Chen, P La Riviere, et al. (2014) Radioluminescence characterization of in situ x-ray nanodosimeters: Potential real-time monitors and modulators of external beam radiation therapy. Appl Phys Lett 105: 203110-203114.
19. RH Krishna, BM Nagabhushana, H Nagabhushana, NS

Murthy, SC Sharma, et al. (2013) Effect of calcination temperature on structural, photoluminescence, and thermo luminescence properties of Y_2O_3: Eu^{3+} nanophosphor. J Phys Chem C 117: 1915-1924.

20. ZH Xu, SS Bian, JQ Wang, T Liu, LM Wang, et al. (2013) Preparation and luminescence of La_2O_3: Ln^{3+} (Ln^{3+} = Eu^{3+}, Tb^{3+}, Dy^{3+}, Sm^{3+}, Er^{3+}, Ho^{3+}, Tm^{3+}, Yb^{3+}/Er^{3+}, Yb^{3+}/Ho^{3+}) microspheres. RSC Adv 3: 1410-1419.

21. Y Gao, J Gong, MM Fan, QH Fang, N Wang, et al. (2012) Large-scale synthesis of Lu_2O_3: Ln^{3+} (Ln^{3+} = Eu^{3+}, Tb^{3+}, Yb^{3+}/Er^{3+}, Yb^{3+}/Tm^{3+} and Yb^{3+}/Ho^{3+}) microspheres and their photoluminescence properties. Mater Res Bull 47: 4137-4145.

22. SA Dalhatu, R Hussin, K Deraman (2016) Structural and luminescence properties of Eu^{3+}-doped magnesium sulfide borate glass and crystal. Chinese J Phys 54: 877-882.

23. WZ Wang, JK Li, ZM Liu (2018) Controlling the morphology and size of $(Gd_{0.98-x}Tb_{0.02}Eu_x)_2O_3$ phosphors presenting tunable emission: Formation process and luminescent properties. J Mater Sci 53: 12265-12283.

24. GC Li, M Lv, J Dai, X Li (2015) Comparative study on two synthesis methods of core-shell structured SiO_2@Y_2O_3: Eu^{3+} particles and their luminescence properties. Opt Mater 46: 40-44.

25. AM Khachatourian, F Golestani-Fard, H Sarpoolaky, C Vogt, MS Toprak (2015) Microwave assisted synthesis of monodispersed Y_2O_3 and Y_2O_3: Eu^{3+} particles. Ceram Int 41: 2006-2014.

26. JK Li, JG Li, XD Li, XD Sun (2016) Tb^{3+}/Eu^{3+} codoping of Lu^{3+}-stabilized $Gd_3Al_5O_{12}$ for tunable photoluminescence via efficient energy transfer. J Alloy Compd 670: 161-169.

27. MY Ding, JJ Hou, ZB Cui, HB Gao, CH Lu, et al. (2018) Bundle-shaped beta-NaYF4 microrods: Hydrothermal synthesis, Gd-mediated downconversion luminescence and ratiometric temperature sensing. Ceram Int 44: 7930-7938.

28. L Liu, HY Li, PY Su, Z Zhang, GR Fu, et al. (2017) Red to white polymer light-emitting diode (PLED) based on Eu^{3+}-Zn^{2+}-Gd^{3+}-containing metallopolymer. J Mater Chem C 5: 4780-4787.

29. D Li, QL Ma, Y Song, X Xi, XT Dong, et al. (2017) A novel strategy to achieve $NaGdF_4$: Eu^{3+} nanofibers with color-tailorable luminescence and paramagnetic performance. J AM Ceram Soc 100: 2034-2044.

30. BJ Park, AR Hong, S Park, KU Kyung, K Lee, et al. (2017) Flexible transparent displays based on core/shell upconversion nanophosphor-incorporated polymer waveguides. Sci Rep 7: 1-7.

31. F Gao, LN Sun, J Tan, XS Li, DY Liu, et al. (2017) Pure and strong red photoluminescence from $Na_{0.5}Gd_{0.5}TiO_3$: Eu ferroelectric thin films under ultraviolet light excitation. Opt Mater 64: 224-229.

32. X Teng, WZ Wang, ZT Cao, JK Li, GB Duan, et al. (2017) The development of new phosphors of Tb^{3+}/Eu^{3+} co-doped $Gd_3Al_5O_{12}$ with tunable emission. Opt Mater 69: 175-180.

33. M Buijs, A Meyerink, G Blasse (1987) Energy transfer between Eu^{3+} ions in a lattice with two different crystallographic sites: Y_2O_3:Eu^{3+}, Gd_2O_3:Eu^{3+} and Eu_2O_3. J Lumin 37: 9-20.

ISSN 2631-5033

DOI: 10.35840/2631-5033/1829

Citation: Li J, Chen Q, Yu H, Cao B, Liu Z (2019) Synthesis and Luminescent Properties of Monodisperse Spherical RE_2O_3:Eu^{3+} (RE = Gd, Y, Lu, La) Phosphors. Int J Earth Sci Geophys 5:029